



**HAL**  
open science

## Growth of $(101\bar{1})$ Semipolar GaN-Based Light-Emitting Diode Structures on Silicon-on-Insulator

Beatrice Wannous, Pierre-Marie Coulon, Ludovic Dupré, Fabian Rol, Névine Rochat, Jesus Zuniga-Perez, Philippe Vennéguès, Guy Feuillet, François Templier

### ► To cite this version:

Beatrice Wannous, Pierre-Marie Coulon, Ludovic Dupré, Fabian Rol, Névine Rochat, et al.. Growth of  $(101\bar{1})$  Semipolar GaN-Based Light-Emitting Diode Structures on Silicon-on-Insulator. *physica status solidi (b)*, 2023, 260 (8), 10.1002/pssb.202200582 . hal-04786121

HAL Id: hal-04786121

<https://hal.science/hal-04786121v1>

Submitted on 15 Nov 2024

**HAL** is a multi-disciplinary open access archive for the deposit and dissemination of scientific research documents, whether they are published or not. The documents may come from teaching and research institutions in France or abroad, or from public or private research centers.

L'archive ouverte pluridisciplinaire **HAL**, est destinée au dépôt et à la diffusion de documents scientifiques de niveau recherche, publiés ou non, émanant des établissements d'enseignement et de recherche français ou étrangers, des laboratoires publics ou privés.



Distributed under a Creative Commons Attribution 4.0 International License

# Growth of (10 $\bar{1}1$ ) Semipolar GaN-Based Light-Emitting Diode Structures on Silicon-on-Insulator

Beatrice Wannous, Pierre-Marie Coulon, Ludovic Dupré, Fabian Rol,\* Névine Rochat, Jesus Zuniga-Perez, Philippe Vennéguès, Guy Feuillet, and François Templier

The growth and characterization of (10 $\bar{1}1$ ) semipolar GaN buffer, InGaN multiple quantum wells (MQWs), and light-emitting diode (LED) structure on patterned silicon-on-insulator (SOI) substrates, implementing the aspect ratio technique (ART), are reported. The early growth stages of GaN result in continuous and uniform stripes with small height variations that cause the formation of chevrons. Three coalescence strategies are tested to improve surface morphology and optical quality. Scanning electron microscopy identifies no crack formation but undulations of the surface. A roughness of  $\approx 10$  nm is measured by atomic force microscopy on large areas. The impact of MQW growth temperature shows similar surface morphology in terms of undulations and roughness. Room temperature photoluminescence spectra show wavelength emission redshifting when decreasing the MQW growth temperature. Room-temperature cathodoluminescence (CL) highlights first the presence of threading dislocations (TDs) in between the coalescence boundary despite the use of the ART technique. Second, CL shows a spatially homogeneous emission wavelength of around 485 nm only perturbed by lower-wavelength emission (455 nm) arising from the chevrons. Blue LED structures exhibit uniform emission wavelength at 450 nm, having a crack-free surface, and roughness of  $\approx 5$  nm. These results pave the way for the fabrication of semipolar micro-LEDs on SOI substrates.

(e.g., liquid crystal displays [LCDs] and organic LEDs) in display applications. Nitride  $\mu$ LEDs also start to show potential in data communication.<sup>[2,3]</sup>

Most of the progress in the development of GaN-based  $\mu$ LEDs is achieved with structures grown along the *c*-direction. However, the electrostatic polarization present along this direction induces a strong internal electric field in the quantum wells. This results in a smaller electron–hole recombination rate within the multiple quantum wells (MQWs) and a wavelength blueshift with the increase in current density, due to the screening of the internal electric field. One of the solutions to avoid or reduce this polarization-induced electric field is the use of nonpolar and semipolar GaN orientation to grow  $\mu$ LEDs on. The electrostatic field along these orientations is reduced, resulting in a higher device efficiency, better wavelength stability with current, and a faster recombination rate.<sup>[4]</sup> These last characteristics can also improve the performance of  $\mu$ LEDs grown along these orientations by decreasing the diffusion length of


the carriers and preventing them from recombining non-radiatively at the sidewalls.<sup>[5]</sup> It is also proved that indium (In) incorporation can be increased by the choice of the crystal orientation, in particular the (10 $\bar{1}1$ ) plane,<sup>[6]</sup> that would allow reaching longer wavelengths.

More recently, both standard LEDs and  $\mu$ LEDs grown on semipolar GaN have demonstrated progress in wavelength stability and lower efficiency droop at high current density.<sup>[7,8]</sup> However,

## 1. Introduction

Indium gallium nitride (InGaN)-based micro-light-emitting diodes ( $\mu$ LEDs) technology has begun to grow and grab the market attention for its promising potential in terms of brightness, efficiency, robustness, color purity, and fast response.<sup>[1]</sup> These characteristics lead to significant enhancement of image quality, creating an opportunity to replace the current technologies

B. Wannous, L. Dupré, F. Rol, N. Rochat, G. Feuillet, F. Templier  
CEA-LETI  
Université Grenoble Alpes  
17 Rue Des Martyrs, 38054 Grenoble, France  
E-mail: fabian.rol@cea.fr

 The ORCID identification number(s) for the author(s) of this article can be found under <https://doi.org/10.1002/pssb.202200582>.

© 2023 The Authors. physica status solidi (b) basic solid state physics published by Wiley-VCH GmbH. This is an open access article under the terms of the Creative Commons Attribution License, which permits use, distribution and reproduction in any medium, provided the original work is properly cited.

DOI: 10.1002/pssb.202200582

P.-M. Coulon, J. Zuniga-Perez, P. Vennéguès  
CRHEA  
CNRS  
Université Côte d'Azur  
06560 Valbonne, France

J. Zuniga-Perez  
MajuLab  
International Research Laboratory IRL 3654  
Sorbonne Université, National University of Singapore, Nanyang Technological University  
138602, Singapore

most of the results are obtained by growing semipolar GaN on either freestanding GaN substrates, which are commercially limited and expensive, or using structured sapphire substrates that have sizes limited to 6".

As an alternative solution, the use of silicon (Si) substrates presents several advantages, the most important one is their commercial availability up to 12". Unfortunately, a high density of defects such as threading dislocations (TDs) and basal stacking faults (BSFs) are associated with the semipolar GaN growth on these foreign substrates, causing a decrease in the device's efficiency. Studies have shown that these defects can be managed using patterned Si substrates, which enable their reduction.<sup>[9]</sup> Another challenge is the impossibility of directly growing GaN on Si due to a violent chemical reaction between Ga and Si, the so-called "meltback etching", that damages the surface. Mantach et al. were able to suppress meltback etching and reduce the TD and BSF densities below  $10^7 \text{ cm}^{-2}$  and  $10^5 \text{ cm}^{-1}$  respectively, by growing (10 $\bar{1}$ 1) semipolar GaN on patterned silicon-on-insulator (SOI) substrate having a top Si(001) with 6° off-axis combined with an aspect ratio trapping (ART) technique.<sup>[10]</sup> This technique consists of using a thick Silicon dioxide (SiO<sub>2</sub>) layer to help block the propagation of the TDs bent by an initial 3D growth. The choice of the SOI substrate with a thin top Si layer is the key to GaN nucleation on a small Si facet allowing the TDs to bend early, as explained by Mantach et al.<sup>[11]</sup> The thick SiO<sub>2</sub> used in ART allows blocking the bent dislocations and prevents them from reaching the surface.

In the current work, we present the development of InGaN-based MQWs and LED structures on patterned ART-SOI substrates made from a 6° off-axis (001) Si layer to obtain a (10 $\bar{1}$ 1) semipolar GaN coalesced layer parallel to the substrate surface. Scanning electron microscopy (SEM) and atomic force microscopy (AFM) are used to investigate surface morphology. Optical

characteristics are studied by cathodoluminescence (CL), photoluminescence (PL), and micro-PL ( $\mu$ PL), which enable to correlate the surface morphology and the defects with the emission wavelength of the MQW and LED structure.

## 2. Experimental Section

The patterning was performed on an SOI substrate made of a 150 nm-thick Si layer on top, whose crystallographic orientation was Si (001) 6° off axis, covered by a thick SiO<sub>2</sub> layer, as presented in **Figure 1a**. First, a buffered oxide etch (BOE) was used to reduce the top SiO<sub>2</sub> layer thickness down to 600 nm (Figure 1b). This SiO<sub>2</sub> thickness was chosen based on the work done by Mantach et al.,<sup>[10]</sup> as it should be thick enough to block the propagation of the bent dislocations. Positive resist deposition was followed by lithography exposure to pattern parallel trenches along Si [110] axis with a periodicity of 5  $\mu$ m (Figure 1c,d). The top SiO<sub>2</sub> was dry etched by inductively coupled plasma (Figure 1e) and then the resist was stripped before wet etching Si by potassium hydroxide (KOH) to reveal the (111) and ( $\bar{1}\bar{1}\bar{1}$ ) facets (Figure 1f). These facets had an angle with the top SiO<sub>2</sub> buffer oxide (BOX) of 60° and 48° respectively. The entire surface was coated by inclined SiO<sub>2</sub> deposition using ion beam sputtering, except for the Si (111) facet where growth took place (Figure 1g). The sample was then introduced in a metal-organic vapor phase epitaxy (MOVPE) 3 × 2" Thomas Swan Close-coupled showerhead reactor for growth of III-nitrides. The used precursors were trimethylaluminum (TMAl), trimethylgallium (TMGa), trimethylindium (TMIn), and ammonia (NH<sub>3</sub>). Prior to GaN growth, a thin aluminum nitride (AlN) layer having a thickness of around 50 nm was grown on the overall surface, resulting in crystalline AlN on the Si (111) facets and polycrystalline AlN on the SiO<sub>2</sub> surface (Figure 1h). The AlN layer helped to prevent meltback

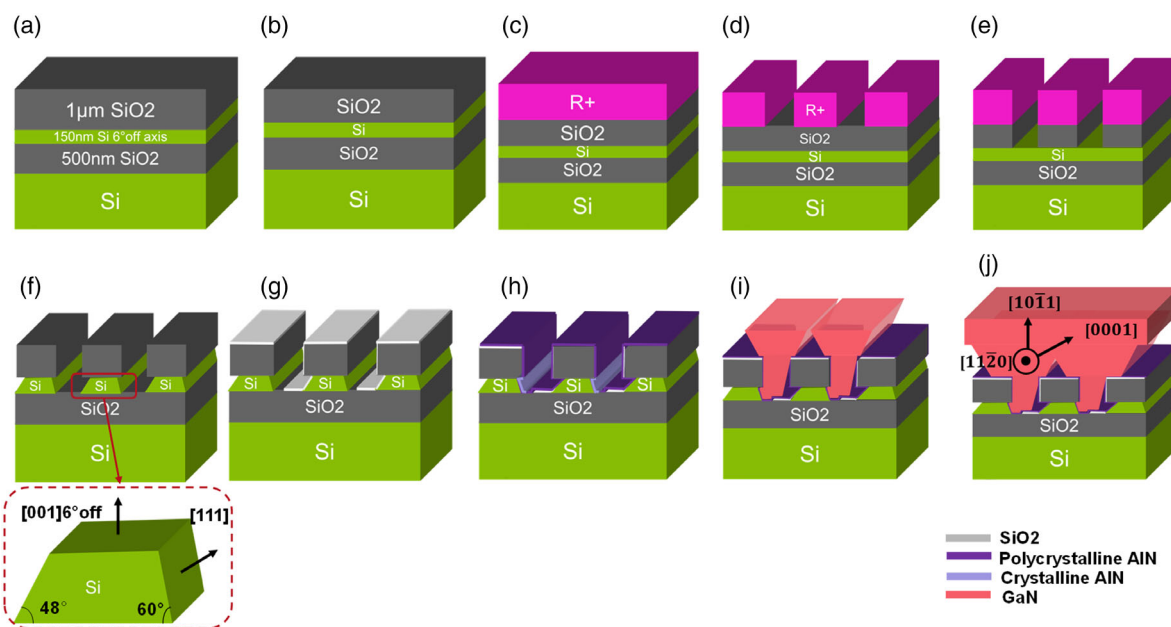


**Figure 1.** Schematic of the different steps of realization of the (10 $\bar{1}$ 1) semipolar GaN buffer. a–g) Patterning of SOI ART substrate and h–j) III-nitride MOVPE growth.

**Table 1.** Summary of the conditions used for each growth step. Note that the temperatures indicated are the set temperatures instead of the measured ones which are  $\approx 100\text{--}150\text{ }^\circ\text{C}$  less.

Growth	Growth conditions		
Step 1: GaN stripes	1140 °C, 300 Torr, 0.156 mol min <sup>-1</sup> NH <sub>3</sub> , 84.450 μmol min <sup>-1</sup> TMGa, 75 min		
Step 2: GaN coalescence	Fully undoped	Fully n-doped	Half undoped/half n-doped
	1120 °C, 100 Torr, 0.067 mol min <sup>-1</sup> NH <sub>3</sub> , 84.450 μmol min <sup>-1</sup> TMGa, 60 min	1160 °C, 100 Torr, 0.312 mol min <sup>-1</sup> NH <sub>3</sub> , 144.771 μmol min <sup>-1</sup> TMGa, 133.9 μmol min <sup>-1</sup> SiH <sub>4</sub> , 60 min	1140 °C, 100 Torr, 0.067 mol min <sup>-1</sup> NH <sub>3</sub> , 84.450 μmol min <sup>-1</sup> TMGa, 30 min + 1160 °C, 100 Torr, 0.312 mol min <sup>-1</sup> NH <sub>3</sub> , 144.771 μmol min <sup>-1</sup> TMGa, 133.9 μmol min <sup>-1</sup> SiH <sub>4</sub> , 30 min
Step 3: InGaN MQW growth	InGaN buffer layer	980 °C	
	InGaN QW	840–820–800 °C	
	GaN barrier/cap	980–960–940 °C	
Step 3 to: LED structure growth	InGaN buffer layer	980 °C	
	InGaN QW	820 °C	
	GaN barrier	960 °C	
	EBL	1140 °C	
	p-GaN	1140 °C	

etching, by isolating the Si surface from the Ga atoms. GaN growth was then carried out in two steps. In step one GaN was grown selectively on AlN/Si (111) to create well-aligned GaN stripes (Figure 1i). Growth conditions allowing selective growth of GaN stripes are given in Table 1. Note that for these conditions no parasitic GaN growth occurred on the polycrystalline AlN. In step two GaN coalescence was initiated in order to obtain a 2D layer (Figure 1j). As n-GaN doped buffer layer will be necessary for subsequent μLEDs processing, we compared three coalescence strategies: 1) an undoped GaN coalescence, as previously used by Mantach et al., 2) a silane (SiH<sub>4</sub>) as n-doped GaN coalescence, and 3) a half undoped/half n-doped GaN coalescence layer. Growth conditions of each strategy are detailed in Table 1. Following coalescence, InGaN-based MQWs containing three QWs were grown on the half undoped/half n-doped GaN coalescence layer. Three set temperatures of 840, 820, and 800 °C were used in order to change the indium composition (see Table 1). Finally, an LED structure was grown: an InGaN temperature of 820 °C was used, followed by a p-AlGaN electron blocking layer (EBL) and a p-doped GaN layer. The conditions for the growth steps are described in Table 1.

The dimensions and surface morphology of grown samples were characterized by SEM using an electron acceleration voltage of 5 keV and by AFM. PL spectra were recorded at room temperature on GaN coalesced layer and on InGaN MQWs using a frequency-doubled argon laser emitting at 244 nm. CL hyperspectral mapping was used at RT with an acceleration voltage of 10 KeV to investigate structural defects, both dislocations and microdefects induced by the growth, as well as to assess their influence on the emission wavelength and intensity homogeneity. Note that the QWs were excited using 10 KeV with a penetration depth of the electron beam in GaN of 600 nm. Finally, μPL mapping was performed on the LED structure using a 405 nm CW Toptica excitation laser, allowing to pump resonantly inside the quantum wells, and a 100× Olympus microscope objective (NA = 0.95 giving a spot size of 300 nm close to the diffraction limit).

## 3. Results and Discussion

### 3.1. GaN Growth

#### 3.1.1. Stripes

Figure 2 displays the GaN stripes after step 1. Figure 2a highlights the selective growth of 2 μm GaN on the AlN on Si (111). No GaN is grown on the 600 nm-thick SiO<sub>2</sub>, while GaN stripe growth propagates on the SiO<sub>2</sub> BOX. The angle between the top pyramid and the substrate is found to be 1.2°. Figure 2b shows the relatively good continuity and uniformity of the stripes after step 1. The growth time is tuned in order to achieve closed packed stripes before modifying the growth conditions for

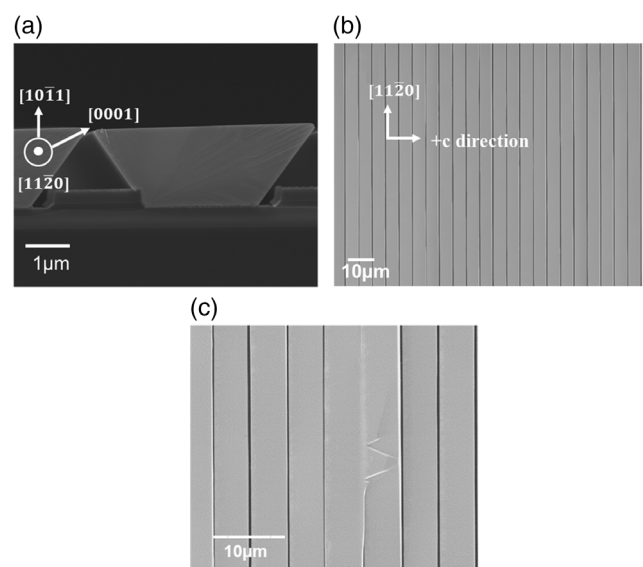


**Figure 2.** a) Cross section and b,c) plan view SEM images of selectively grown GaN stripes on AlN/Si (111).

initiating coalescence. This has been found to further mitigate meltback etching. Note that scarce nonuniformities in the width of the stripes can be observed, resulting in two stripes being partially coalesced, as displayed in Figure 2c. In that case, we observe the early formation of triangular features, so-called chevrons.<sup>[12]</sup>

The formation of chevrons seems to be related to an imperfect coalescence where a stripe climbs over a neighboring one due to small height differences between neighboring stripes, which agrees with other reports as well for different GaN orientations.<sup>[13]</sup> Additional fluctuations in height along one stripe and or local defect could explain why these chevrons appear on isolated regions and not along the whole coalesced length. More in-depth characterization is underway to understand their formation. Their impact on InGaN QW growth will be discussed later.

### 3.1.2. Coalescence

The morphologies of the three GaN coalescence strategies are observed by tilted SEM and presented in Figure 3.

After 60 min and around 2  $\mu\text{m}$  of undoped GaN coalescence, Figure 3a reveals a large density of chevrons at the surface. After 60 min of n-doped GaN coalescence. Figure 3b shows the presence of parasitic growth (highlighted in red) as well as uncoalesced stripes. The use of completely different growth conditions between undoped and n-doped GaN can explain these two types of features. Indeed, higher temperature and higher  $\text{NH}_3$  flow rate used for the n-doped GaN will favor parasitic nucleation on the BOX and will decrease growth along the  $c$ -direction, respectively, and hence prevent coalescence. Interestingly, 30 min of undoped GaN followed by 30 min of n-doped GaN, for a total thickness around 2  $\mu\text{m}$ , shows an improved surface morphology, with a lower density of chevrons (Figure 3c). Such improvement can be explained by a complete coalescence after 30 min of undoped GaN followed by n-doped GaN growth at

higher temperature, which enables to smooth out the surface. AFM was carried out on the last layer. Figure 3d displays a  $10 \times 10 \mu\text{m}^2$  map which reveals root mean square (RMS) roughness of  $\approx 10$  nm. Note that this roughness does not take into account the chevron features, which would increase further the measured roughness. Chiu et al. demonstrated a correlation between the formation of chevrons (or step-like structure) with the associated large roughness and the exact Si (001) substrate misorientation. They measured a GaN roughness of 5.9 nm on Si (001) with  $6.5^\circ$  off axis compared to 0.7 nm roughness on  $7^\circ$  off axis when coalescing with undoped GaN.<sup>[14]</sup> Similarly, it was shown that  $(10\bar{1}1)$  GaN surface with roughness below 1 nm can be obtained on  $(11\bar{2}3)$   $\text{Al}_2\text{O}_3$  for which an angle of  $61.22^\circ$  is obtained with respect to  $c$ -plane sapphire, close to that of  $61.96^\circ$  between the  $\{10\bar{1}1\}$  plane of GaN and the  $c$ -plane of GaN.<sup>[15,16]</sup> This suggests that fine tuning the initial Si (001) off axis orientation can further improve the surface morphology of the GaN coalesced layer.

Figure 4 presents the PL spectra of the three GaN coalesced layers. The GaN near-band-edge (NBE) emission is observed at 360 nm while the yellow band (YB) emission, often ascribed to point defects, is centered around 550 nm.<sup>[17]</sup> Intensities of the NBE increase with the increase of doping concentration due to nonradiative transitions dominating the undoped GaN.<sup>[18]</sup> The ratio between the NBE and the YB intensities is found to be smaller for both  $\text{SiH}_4$ -doped samples compared to the undoped GaN, which can be attributed to the substitution of Ga vacancies by Si dopants.<sup>[19]</sup> The half-undoped/half-doped GaN coalesced layer displays the best optical properties probably due to a combination of improved structural quality and the higher radiative recombination rate of the n-doped section. Consequently, three MQWs were grown on templates made of two sections (30 min undoped and 30 min n-doped sample), as they showed better structural and optical properties.

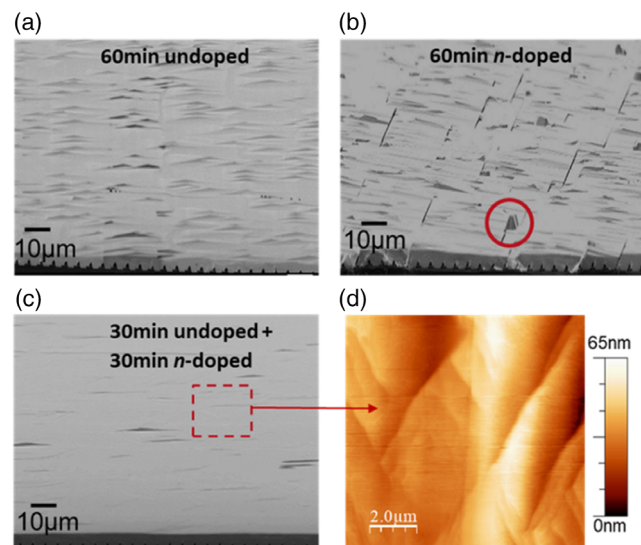


**Figure 3.** Tilted SEM images of GaN coalesced layer after a) 60 min undoped, b) 60 min n-doped (red circle highlighting the parasitic growth), and c) 30 min undoped/30 min n-doped growth. d)  $10 \times 10 \mu\text{m}^2$  AFM image of sample in (c).

### 3.2. MQW Growth and Optical Characterization

SEM images in Figure 5a–c display similar surface features after MQW growth, irrespective of the MQW growth temperature (from 840 to 800  $^\circ\text{C}$ ). The surface reveals the complete absence

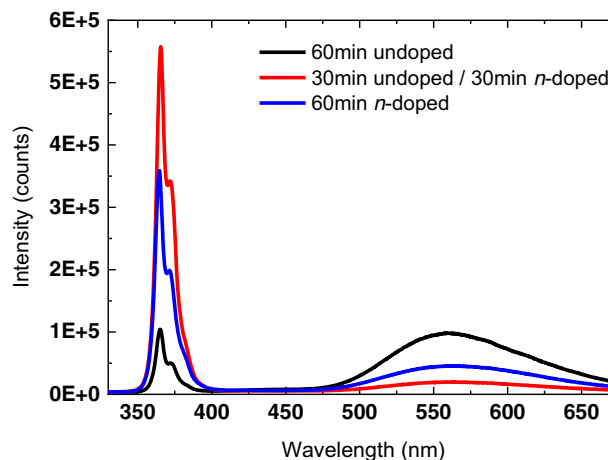


**Figure 4.** RT PL spectra of the three GaN coalesced layers.

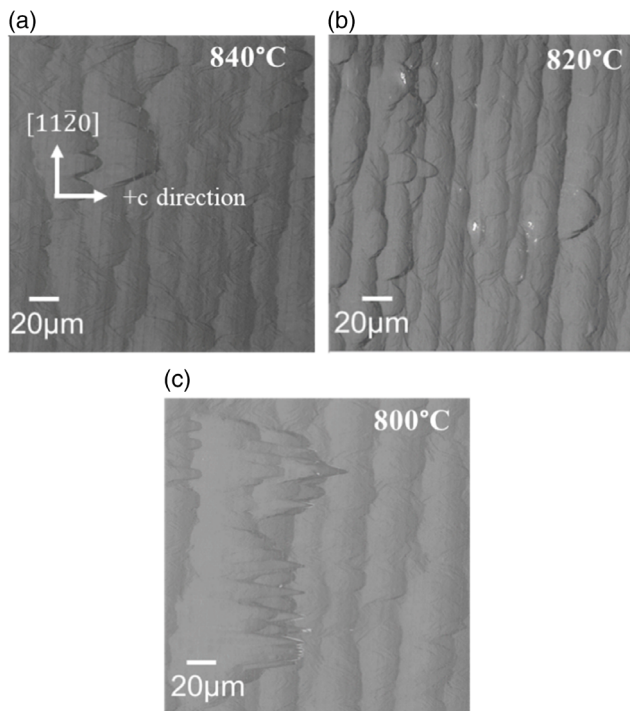


**Figure 5.** Plan-view SEM images of the MQW grown at a) 840 °C, b) 820 °C, and c) 800 °C.

of cracks, some undulations along the +c direction, and the presence of chevrons.

The formation and presence of chevrons have already been discussed earlier. However, it is worth mentioning that the evolution of their dimensions could be further impacted by the lower growth temperature used for the QWs and the GaN barrier/cap.

Meanwhile, the emergence of well-defined undulations could have two potential explanations. The first could be related to anisotropic surface diffusion between the  $[10\bar{1}1]$  direction and the +c-direction, which has already been reported for different directions in  $(11\bar{2}0)$  GaN layers grown on  $(11\bar{2}0)$  bulk GaN substrates. A lower growth temperature, used for the QWs and the GaN barrier/cap, could then further enhance the anisotropic surface diffusion between the two directions and trigger the formation of periodic undulations. A second explanation could be the initial imperfect coalescence, triggering periodic undulations after GaN coalescence, which would be then further exacerbated at lower temperatures. Note that the periodicity of the aforementioned undulations seems to vary between the samples but is always larger than the initial 5 µm period of the patterned stripes.

**Figure 6** shows the RT PL spectra of the three different MQWs grown at different temperatures. It clearly shows that when decreasing the temperature from 840 to 800 °C, the InGaN emission redshifts from 430 to 490 nm. Indium incorporation is sensitive to growth temperature because of In evaporation from the surface at higher temperatures during growth, hence the higher In composition while decreasing the MQW temperatures. In addition, we only observe a slight decrease in intensity with the temperature, which might be ascribed to the quality degradation when incorporating more indium.<sup>[20]</sup> However, we need

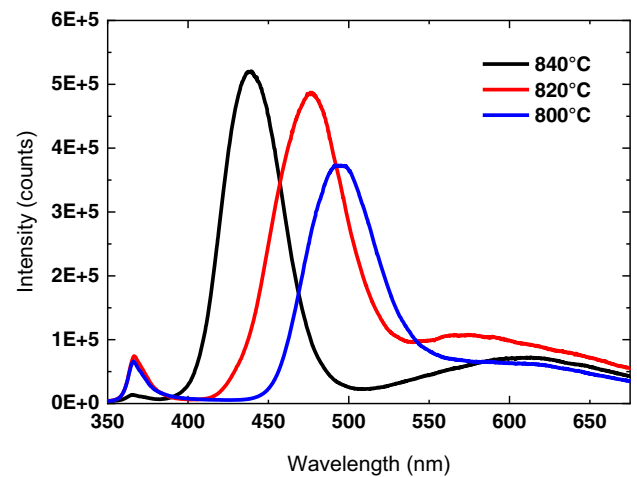


**Figure 6.** RT PL spectra of the three samples having MQW grown at 840, 820, and 800 °C.

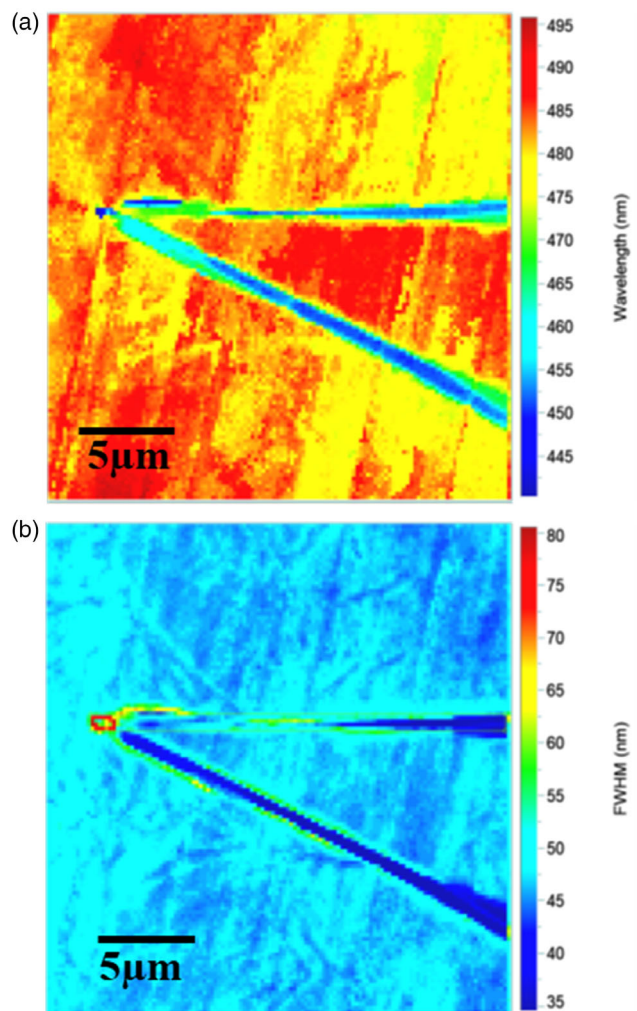


**Figure 7.** RT CL map of the a) wavelength peak position and b) FWHM of the QW emission for the sample grown at 800 °C.

to be careful with absolute PL intensity comparison, as light extraction can vary from one sample to another, for example, due to a possible small change of density of large defects like chevrons, that will induce more or less light scattering.

**Figure 7** presents RT CL acquisition performed around a chevron feature for the MQWs grown at 800 °C.

The map of the wavelength peak position in **Figure 7a** indicates a relatively low-wavelength dispersion of  $485 \pm 10$  nm on the flat area surrounding the chevron and on its top. The arms of the chevron are instead dominated by lower-wavelength emission at  $455 \pm 15$  nm. This could be due either to lower In incorporation or to a variation of the well widths along the different GaN plane orientations on the chevron arms. The full width at half maximum (FWHM) map of the QW emission indicates a broadening in the order of  $50 \pm 5$  nm, which becomes narrower within the chevrons arms (**Figure 7b**). Both results highlight the chevron's impact on the resulting QW wavelength emission and broadening, which was also observed by Brassier et al.<sup>[12]</sup>

### 3.3. Strategies for Further Improvements

RT CL integrated intensity map of the GaN NBE is illustrated in **Figure 8a**. It shows two distinguishable areas: one with high TD density, along the coalescence boundary of two consecutive

stripes (red arrow), and a region with a lower density of TDs in between coalescence boundaries (white bracket).

Note that although not investigated in this article, the BSF density should be similar to the one observed by Mantach et al. for ART-SOI substrates ( $\approx 10^4 \text{ cm}^{-1}$ ).<sup>[10]</sup> As schematically displayed in **Figure 8b**, BSFs are located in the small  $-c$ -grown regions (purple lines) which end up being close to the coalesce boundary where dislocations are generated.

The purpose of using a thick SiO<sub>2</sub> layer on top of the Si is to implement the ART strategy. However, one should note that for the ART to operate in the semipolar geometry, dislocations should bend laterally during early growth. Indeed, when TDs meet an inclined facet, they will bend at 90° (i.e., into the basal plane), as schematically depicted in **Figure 8b**. If the pyramidal GaN stripe is fully formed in the early growth, as represented on the left side of **Figure 8b**, all dislocations will bend and will be trapped by the thick SiO<sub>2</sub>. On the contrary, if the pyramidal GaN stripe is truncated, as schematically shown in **Figure 8b** on the right side, TDs can propagate and bend at a later stage with a reduced effect of the thick SiO<sub>2</sub>. **Figure 8c** shows an SEM cross section of GaN stripes after step 1, where the formation of truncated (red circle) and fully formed (green circle) pyramidal GaN stripes can be observed. This seems to confirm the origin of the unexpected dislocation lines away from the coalescence areas (indicated by a white arrow in **Figure 8a**).

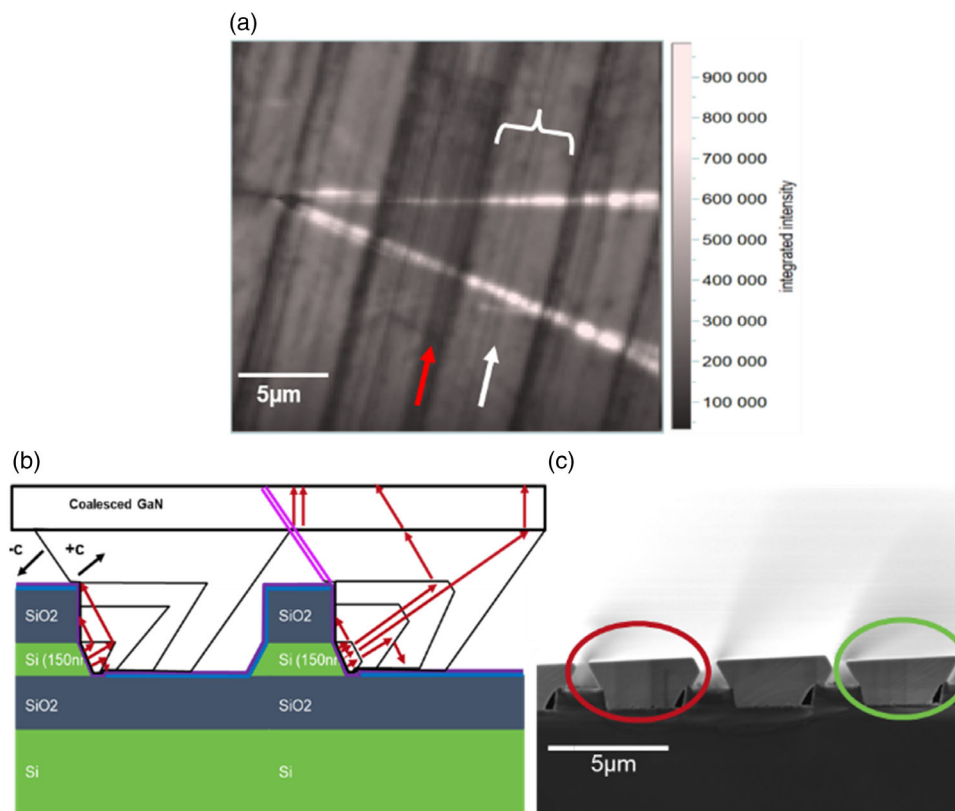


**Figure 8.** a) RT CL NBE-integrated intensity image indicating a high TD density with a red arrow and a low one with a white arrow. b) A scheme representing the propagation of TDs (red arrows) and the presence of BSFs (purple lines) at the coalescence boundary, in addition to showing the difference between complete and truncated pyramids resulting in different dislocations blocking; c) a 10° tilt cross-section SEM image of complete and truncated pyramids highlighted by green and red circles respectively.

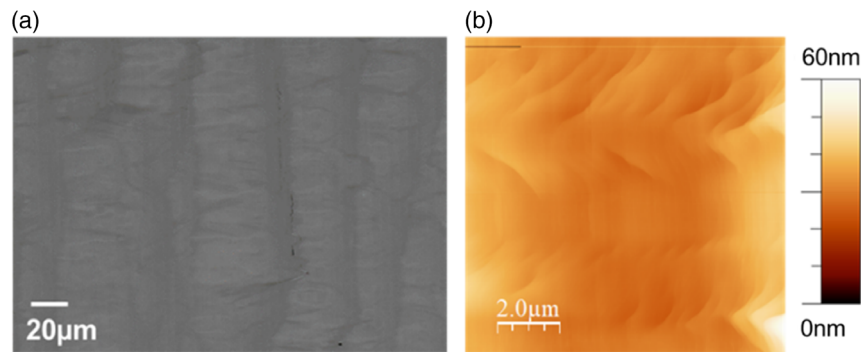


**Figure 9.** a) Plan-view SEM image and b) a  $10 \times 10 \mu\text{m}^2$  AFM image of the LED sample.

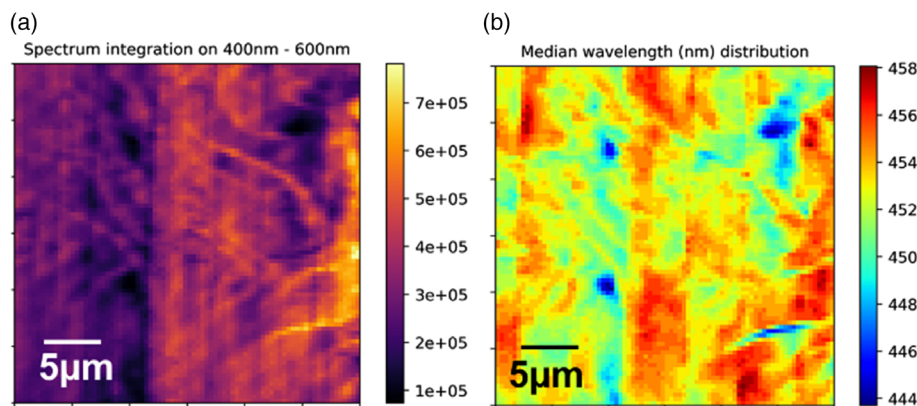


**Figure 10.** a)  $\mu\text{PL}$  intensity map and b) wavelength peak position map acquired on the same area of the LED sample with MQWs at  $820^\circ\text{C}$ .

In order to tackle these problems and further reduce the dislocation density, the formation of GaN stripes in step 1 should be optimized in order to create only well-defined pyramids in the early growth stages.

### 3.4. LED Growth Structure

Plan-view SEM image and AFM measurements shown in **Figure 9a, b**, respectively, indicate a similar surface morphology to the one of the MQW structure in terms of undulations, but with an improved surface roughness ( $<5 \text{ nm}$ ). Besides, even if the total thickness of the LED structure is around  $4 \mu\text{m}$ , no cracks are observed.

**Figure 10a, b** shows  $\mu\text{PL}$  intensity and wavelength map of the LED structure, respectively, indicating homogenous intensity along the surface and a uniform emission wavelength around  $450 \text{ nm}$ , despite the observed surface features. The emission wavelength shift between MQWs and LED structure (around  $25 \text{ nm}$ ) for the same MQW growth temperature might be attributed to the indium interdiffusion occurring in the MQWs when subsequent layers are grown at a higher temperature.

## 4. Conclusion

We have reported the growth and characterization of  $(10\bar{1}1)$  semipolar GaN templates on patterned off-axis SOI substrates,

while implementing the ART technique. Despite the uniform and continuous GaN stripes obtained after the first growth step, a local height difference between the stripes has led to the formation of chevron features.  $(10\bar{1}1)$  GaN templates having no cracks, a good structural and optical quality, and a relatively low surface roughness were then achieved by combining undoped and Si-doped GaN for 2D coalescence. The latter is known to be necessary for the LED structure. Subsequent growth of three QWs and an LED structure were also achieved on these templates.

SEM showed a similar surface morphology for the MQW growth as the GaN template in terms of undulations, no cracks, nor meltback etching and roughness of  $\approx 10 \text{ nm}$ . A change in the MQWs temperature shows a clear shift toward longer wavelengths from  $430$  to  $490 \text{ nm}$ . CL highlighted the effect of the chevrons morphology on the wavelength emission and, second, indicated the propagation of dislocations despite the use of the ART technique, whose origin has been elucidated. Finally, a blue semipolar LED structure was achieved with a similar surface morphology as the MQW structures and a uniform wavelength emission at  $450 \text{ nm}$ .

These results constitute a demonstration of all necessary building blocks to fabricate a semipolar LED epistructure that will be key in the near future for the realization of semipolar  $\mu\text{LEDs}$ .



## Conflict of Interest

The authors declare no conflict of interest.

## Data Availability Statement

The data that support the findings of this study are available from the corresponding author upon reasonable request.

## Keywords

growth, InGaN multiple quantum wells, LED structures, light-emitting diodes, micro-LEDs, semipolar GaN, silicon-on-insulator substrates

Received: November 30, 2022

Revised: February 16, 2023

Published online: March 18, 2023

- 
- [1] J. Y. Lin, H. X. Jiang, *Appl. Phys. Lett.* **2020**, *116*, 100502.  
[2] Z. Chen, S. Yan, C. Danesh, *J. Phys. D: Appl. Phys.* **2021**, *54*, 123001.  
[3] B. Pezeshki, A. Tselikov, C. Danesh, R. Kalman, in *2021 European Conf. Optical Communication (ECOC)*, Bordeaux, France **2021**, pp. 1–3.  
[4] S.-H. Park, S.-L. Chuang, *Phys. Rev. B* **1999**, *59*, 4725.  
[5] A. David, *Phys. Rev. Appl.* **2021**, *15*, 054015.  
[6] Y. Zhao, Q. Yan, C.-Y. Huang, S.-C. Huang, P. Shan Hsu, S. Tanaka, C.-C. Pan, Y. Kawaguchi, K. Fujito, C. G. Van de Walle, J. S. Speck, S. P. DenBaars, S. Nakamura, D. Feezell, *Appl. Phys. Lett.* **2012**, *100*, 201108.  
[7] M. Monavarian, A. Rashidi, D. Feezell, *Phys. Status Solidi A* **2018**, *216*, 1800628.  
[8] S.-W. H. Chen, Y.-M. Huang, K. J. Singh, Y.-C. Hsu, F.-J. Liou, J. Song, J. Choi, P.-T. Lee, C.-C. Lin, Z. Chen, J. Han, T. Wu, H.-C. Kuo, *Photonics Res.* **2020**, *8*, 630.  
[9] M. Khoury, P. Vennéguès, M. Leroux, V. Delaye, G. Feuillet, J. Zúñiga-Pérez, *J. Phys. D: Appl. Phys.* **2016**, *49*, 475104.  
[10] R. Mantach, P. Vennéguès, J. Zuniga-Perez, P. De Mierry, M. Portail, G. Feuillet, *Appl. Phys. Express* **2020**, *13*, 115504.  
[11] R. Mantach, P. Vennéguès, J. Z. Perez, P. De Mierry, M. Leroux, M. Portail, G. Feuillet, *J. Appl. Phys.* **2019**, *125*, 035703.  
[12] C. Brasser, J. Bruckbauer, Y. Gong, L. Jiu, J. Bai, M. Warzecha, P. R. Edwards, T. Wang, R. W. Martin, *J. Appl. Phys.* **2018**, *123*, 174502.  
[13] M. Caliebe, Y. Han, M. Hocker, T. Meisch, C. Humphreys, K. Thonke, F. Scholz, *Phys. Status Solidi B* **2016**, *253*, 46.  
[14] C.-H. Chiu, D.-W. Lin, C.-C. Lin, Z.-Y. Li, Y.-C. Chen, S.-C. Ling, H.-C. Kuo, T.-C. Lu, S.-C. Wang, W.-T. Liao, T. Tanikawa, Y. Honda, M. Yamaguchi, N. Sawaki, *J. Cryst. Growth* **2011**, *318*, 500.  
[15] S. Schwaiger, I. Argut, T. Wunderer, R. Röscher, F. Lipski, J. Biskupek, U. Kaiser, F. Scholz, *Appl. Phys. Lett.* **2010**, *96*, 231905.  
[16] M. Takami, A. Kurisu, Y. Abe, N. Okada, K. Tadatomo, *Phys. Status Solidi C* **2011**, *8*, 2101.  
[17] J. Neugebauer, C. G. Van de Walle, *Appl. Phys. Lett.* **1996**, *69*, 503.  
[18] E. F. Schubert, I. D. Goepfert, W. Grieshaber, J. M. Redwing, *Appl. Phys. Lett.* **1997**, *71*, 921.  
[19] F. Qian, G. Xin, Z. Xiao-Ju, H. Yue, *Chin. Phys.* **2005**, *14*, 2133.  
[20] S. T. Pendlebury, P. J. Parbrook, D. J. Mowbray, D. A. Wood, K. B. Lee, *J. Cryst. Growth* **2007**, *307*, 363.